AGU PUBLICATIONS

Geophysical Research Letters

RESEARCH LETTER
10.1002/2014GL061170

Key Points:
- We document the first GPS time series of a landslide response to an earthquake
- The landslide response is not purely coseismic but lasts for 5 weeks
- We show the mechanical analogy of slow-moving landslides and creeping faults

Supporting Information:
- Readme
- Text S1

Correspondence to:
P. Lacroix,
pascal.lacroix@ujf-grenoble.fr

Citation:
Lacroix, P., H. Perfettini, E. Taipe, and B. Guillier (2014), Co- and Postseismic motion of a landslide; observations, modelling and analogy with tectonic faults, *Geophys. Res. Lett.*, *41*, 6676–6680, doi:10.1002/2014GL061170.

Received 10 JUL 2014
Accepted 11 SEP 2014
Accepted article online 13 SEP 2014
Published online 1 OCT 2014

Coseismic and postseismic motion of a landslide: Observations, modeling, and analogy with tectonic faults

P. Lacroix[1,2,3], H. Perfettini[1,2,3], E. Taipe[4], and B. Guillier[1,2,3]

[1]ISTerre, Université Grenoble Alpes, Grenoble, France, [2]CNRS, ISTerre, Grenoble, France, [3]IRD, ISTerre, Grenoble, France, [4]NGEMMET, Arequipa, Peru

Abstract We document the first time series of a landslide reactivation by an earthquake using continuous GPS measurements over the Maca landslide (Peru). Our survey shows a coseismic response of the landslide of about 2 cm, followed by a relaxation period of 5 weeks during which postseismic slip is 3 times greater than the coseismic displacement itself. Our results confirm the coseismic activation of landslides and provide the first observation of a postseismic displacement. These observations are consistent with a mechanical model where slip on the landslide basal interface is governed by rate and state friction, analogous to the mechanics of creeping tectonic faults, opening new perspectives to study the mechanics of landslides and active faults.

1. Introduction

The mechanics of landsliding under seismic forcing assume that the landslide kinematics can be modeled by the perturbation of the basal friction of a rigid block moving on a sliding surface [*Newmark*, 1965]. This model suggests a pure coseismic motion, but various observations suggest a more complicated mechanism. Delayed initiation ranging from hours to days after the earthquake are sometimes observed [*Hadley*, 1960; *Jibson et al.*, 1994; *Keefer*, 2002; *Agnesi et al.*, 2005] and cannot be explained by coseismic effects only. Also, earthquakes can produce numerous fissures that accelerate the rate of landslides during the subsequent heavy rains [*Lin et al.*, 2008; *Huang and Fan*, 2013]. These postseismic effects have been explained by coseismic weakening of substrate material [*Dadson et al.*, 2004; *Petley et al.*, 2006] or increased spring flow and pore water pressures associated with tectonic deformation [*Jibson et al.*, 1994; *Wasowski et al.*, 2002]. However, all these assumptions have never been validated considering geodetic data acquired on active landslides during an earthquake. Unfortunately, these data are sparse [*Wilson and Keefer*, 1983; *Jibson et al.*, 1994; *Harp and Jibson*, 1995; *Pradel et al.*, 2005; *Moro et al.*, 2011] and lack the temporal resolution required to correctly distinguish the coseismic from the preseismic and postseismic effects.

To increase our understanding of the triggering mechanisms of landslides by earthquakes, we studied the Maca landslide, situated in the central volcanic zone of Peru (Figure 1), an area of intense sustained seismicity [*Dorbath et al.*, 1990; *Antayhua et al.*, 2002]. This landslide is a slow-moving translational slide [*Cruden and Varnes*, 1996] that developed into lacustrine sediments. Rainfall is the main factor of instability, with a seasonal movement related to the binary seasons of the Andean fore-arc region (Figure 2). The particularity of this landslide is the sensitivity of the movement to earthquakes, with several reactivations occurring in 1991 and 2001 after tectonic earthquakes [*Bulmer et al.*, 1999; *Gomez et al.*, 2002].

On 17 July 2013, a shallow M_w 6.0 earthquake struck the Colca region, south of Peru. The location and induced surface deformation of this earthquake is known by the interferometric synthetic aperture radar (InSAR) processing represented in Figure 1. The Maca landslide, 20 km far from this earthquake, is located outside the region of significant deformation. A continuous GPS station, installed on the active part of the landslide (Figure 1b) on an area representative of the overall landslide motion (except its northern part where the river erosion plays a major effect), recorded the triggered movement (Figure 2). The occurrence of this earthquake is a real opportunity to study landslide dynamics under seismic forcing. Indeed, it occurred during the dry season (Figure 2) so that the effects of rainfalls and earthquake on the landslide movement can easily be decoupled.

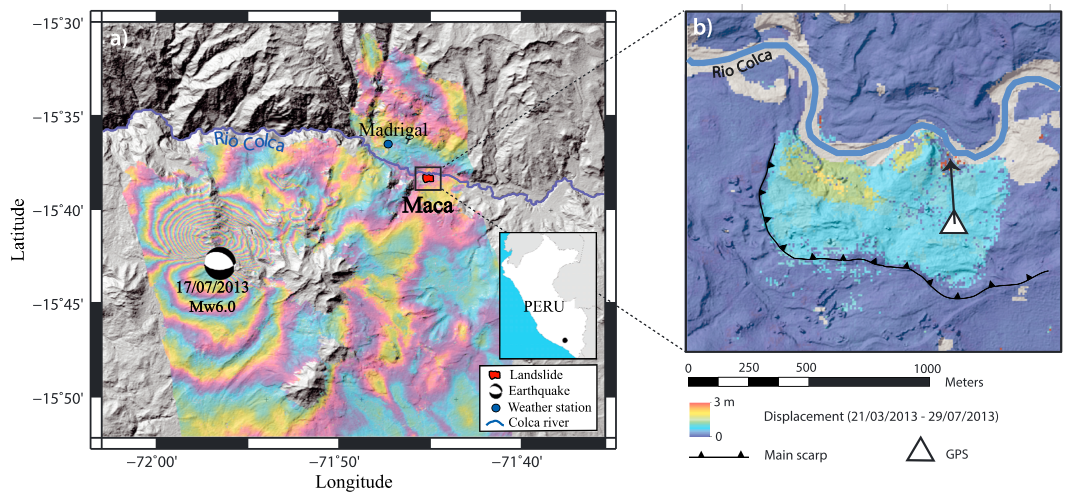

Figure 1. (a) Map of the Colca valley and (b) zoom on the landslide area. The deformation field produced by the 17 July 2013 M_w 6.0 earthquake is represented in color levels based on an InSAR of TerraSAR-X data (Copyright Deutsches Zentrum für Luft-und Raumfahrt 2013, courtesy of J. Jay) (Figure 1a). Each fringe cycle represents 1.6 cm change in the line of sight between the satellite and the surface. The position of the permanent GPS is replaced on the deformation field (21 March 2013 to 29 July 2013) of the Maca landslide, estimated by correlation of two successive orthorectified Pléiades images (Copyright Centre National d'Etudes Spatiales 2013/Distribution Airbus Defence and Space) on windows of 64 pixel size (Figure 1b). Areas where the correlation coefficient is lower than 0.95 are represented in gray.

2. Data and Methods

The GPS data analyzed, with a sampling frequency of 15 s, cover the preseismic, coseismic, and postseismic period over 6 months. The data are processed both statically on 24 h sessions for the whole period and kinematically at a 15 s sampling rate for the day of the earthquake.

The 24 h sessions GPS data were processed using the GAMIT/GLOBK software [*Herring et al.*, 2010], with 33 International Global Navigation Satellite Systems Service (IGS) stable points situated in South America and the Pacific Ocean. The baselines between all GPS points were first calculated by least squares adjustment for each 24 h session (GAMIT). The time series (Figure 3) for each point were then calculated in the International Terrestrial Reference Frame referential [*Altamimi et al.*, 2012] by optimization using Kalman filters (GLOBK). Then, to remove unmodeled errors, we subtract the IGS Arequipa GPS time series (situated 70 km far from the site) from the landslide GPS time series. Uncertainties are 1 mm in horizontal, 4 mm in vertical, as estimated by formal means from the GLOBK solution.

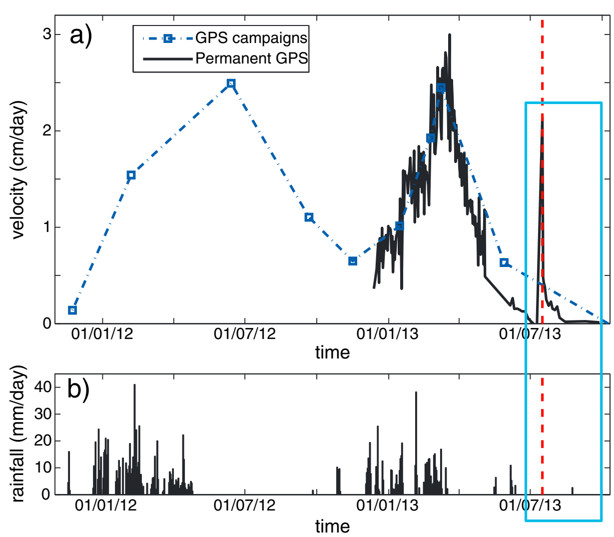

Figure 2. Time series of (a) GPS velocities and (b) rainfalls. Figure 2a represents the velocity over 2 years, based on either campaigns (blue) or permanent GPS (black) measurements. The timing of the 17 July 2013 earthquake is represented with the red dotted line. The blue box refers to the zoom presented on Figure 3.

For better quantification of the movement during the earthquake, a precise point positioning (PPP) kinematic processing [*Zumberge et al.*, 1997] has been undertaken at a 15 s rate for the day of the earthquake (Figure 3, inset), using the Canadian Spatial Reference System

10.1002/2014GL061170

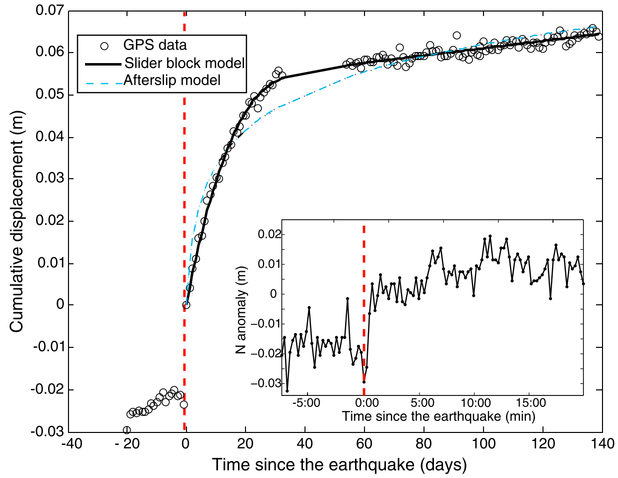

Figure 3. Time series of the Maca GPS cumulative displacement amplitude relatively to Arequipa at a 1 day sampling rate using a static processing and zoom (inset) on the north component around the earthquake timing processed at a 15 s sampling rate using a kinematics processing. The best fits using the afterslip and gravity models are represented with blue and black curves, respectively. The red vertical bar represents the timing of the 17 July 2013 earthquake.

(CSRS)-PPP online application. The uncertainties were estimated as the standard deviation of the time series on a 30 min time window before the earthquake, leading to uncertainties of 6 mm in both horizontal directions and 1 cm on the vertical. Finally, the coseismic offsets are estimated for each east, north, and up component by difference of the mean values of the time series calculated on a 10 min time window before and after the earthquake.

The GPS time series show a coseismic displacement offset, followed by a postseismic relaxation for about 35 days and a return to a steady state velocity (Figures 2 and 3). The coseismic displacement (Figure 3) of 2 ± 0.6 cm northward and 0.8 ± 1 cm downward is fully consistent with the direction of the landslide displacement calculated by 2 years of GPS campaigns (azimuth N2°, dip 15°). The postseismic motion (Figure 3), with about 6 cm of cumulative displacement, is 3 times greater than the coseismic one. It displays a logarithmic increase for about 35 days, followed by a return to a steady state velocity $V_L = 8.67\ 10^{-5}$ m/d (3.1 cm/yr).

3. Discussion

The coseismic movement of the Maca landslide compares well with other studies showing coseismic landslide displacement of few centimeters after M_w 6.3–6.7 earthquakes for source-to-landslide distances between 10 and 25 km [*Pradel et al.*, 2005; *Moro et al.*, 2011]. The initiation of the accelerating phase is clearly triggered by the shaking of the seismic waves (Figure 3, inset). The coseismic displacement is found to be accommodated within about 30 s, which is approximately the duration of the soft soil ground motion for a M_w 6.0 earthquake at 20 km distance [*Trifunac and Brady*, 1975]. This coseismic observation therefore confirms the dynamic triggering of this landslide as assumed by previous studies [e.g., *Newmark*, 1965].

The postseismic motion of landslides observed here has, however, never been quantified. In particular, the shape of the landslide response to the earthquake shaking is very intriguing and raises the question of the mechanisms of landsliding under seismic forcing. Since no variations of the river flow nor a delayed response of the motion are observed, destabilization by increase of the water pore pressure can be discarded [*Wang et al.*, 2001]. A more appealing mechanism would be variations of the frictional stress of the interface due to a sudden increase of the sliding velocity induced by the passage of seismic waves [*Chau*, 1995]. Indeed, the response of the Maca landslide to nearby earthquakes resembles the postseismic response of a tectonic fault to a coseismic slip: (1) a sudden motion due to the main shock followed by (2) a relaxation during which slip rate decays to reach its long-term value V_L.

Following this analogy, one can first consider the model of *Perfettini and Avouac* [2004] that describes the evolution of the postseismic slip following a main shock under the assumption that friction on the creeping patch is governed by rate and state friction [*Dieterich*, 1981]. In this model, the elastic response of the medium plays a fundamental role since only a fraction of the interface is sliding, the rest of the interface remaining locked. A second major difference is that no inertial terms are needed in this model. We will refer to this model, described in the supporting information, as the afterslip model. The main parameters of this model are V_L, V^+, the sliding velocity at the end of the coseismic phase, and t_r, the relaxation time. If the whole interface of the landslide is sliding homogeneously, then the elastic response of the medium can be ignored, and the landslide can be described as a block sliding under its own weight, analogous to the slider block model of *Newmark* [1965]. We will refer to this model, presented in the supporting information, as the slider block model. The slope of the sliding interface (≈ 15°) is inferred from the GPS measurements. The free parameters of the model are the frictional parameters d_c, a, and b and the velocities V_L and V^+. To evaluate the goodness of the fit to the models presented here, we use a reduced chi-square criterion χ_r (see the supporting information).

Figure 3 shows the evolution of the total slip with time. When the afterslip model is considered, the best fit to the data yields $V_L = 1.04\,10^{-6}$ m/d, $V^+ = 1.91\,10^{-1}$ m/d, and $t_r = 1.53\,10^5$ days. The model fails to adjust properly the data, and $\chi_r^2 \approx 0.41$. So we reconsider the assumption that only a fraction of the interface is sliding and suppose that the whole interface is slipping as in the slider block model. The best fit to the data using the slider block model leads to $d_c = 6.12\,10^{-5} \pm 1.59\,10^{-6}$ m, $a = 4.37\,10^{-5} \pm 2.96\,10^{-7}$, $b = 3.96\,10^{-5} \pm 4.10\,10^{-7}$, $V_L = 8.50\,10^{-5} \pm 8.43\,10^{-6}$ m/d, and $V^+ = 3.60\,10^{-3} \pm 8.59\,10^{-5}$ m/d. The model adjusts the data perfectly (Figure 3), and $\chi_r^2 \approx 4.78\,10^{-2}$. Although formally five parameters need to be adjusted, the values of the dynamic parameters V_L and V^+ of the best fit model are in close agreement with the observed values so that in practice, the only relevant parameters are the frictional parameters a, b, and d_c.

Laboratory values of d_c typically fall in the range 10^{-6}–10^{-5} for dry surfaces but can be much larger when fault gouge is considered [*Marone*, 1998], making our estimate of d_c consistent with those estimates. The ratio $a/b \approx 1.1$ is consistent with rate-strengthening friction ($a/b > 1$). The difference $a - b$ is smaller than laboratory estimates on natural clay-rich fault samples which typically stands in the range 10^{-4}–10^{-2}. A decrease of $a - b$ with the loading velocity and confining pressure has been observed in laboratory experiments [*Saffer et al.*, 2001; *Ikari et al.*, 2009; *Boulton et al.*, 2012, 2014; *Niemeijer and Vissers*, 2014]. We believe that our low estimate of $a - b$ ($\simeq 4 \times 10^{-6}$) is consistent with the much lower loading velocity of the landslide, estimated to be of the order of 10^{-9} m/s, a value at least 2 orders of magnitude lower than the loading velocities in those experiments. Our low estimate of $a - b$ is also consistent with the lower effective normal stress on the landslide interface (of the order of 0.5 MPa, assuming a stress gradient of 10 kPa/m and a thickness of the landslide body of 50 m), compared to the typical 100 MPa for laboratory experiments. The ratio $V^+/V_L \approx 42$ is smaller than inferred from the analysis of postseismic slip following large earthquakes [*Perfettini and Avouac*, 2004; *Hsu et al.*, 2006]. This is not surprising remembering that the stress changes experienced by the Maca landslide, distant by about 20 km from the main shock (two fault lengths), are much smaller than those experienced by creeping zones immediately surrounding the areas of coseismic rupture.

4. Conclusion

Based on a unique data set of GPS measurements over a landslide during a M_w 6.0 earthquake at source-to-site distance of 20 km, we confirm the dynamic triggering of landslides during earthquakes and show the first evidence of a landslide postseismic movement. Our modeling suggests that the mechanisms of landsliding can be treated as a rigid body, equivalent in assuming that the whole interface is sliding homogeneously under rate and state dependent friction. Even though the slider block model has been applied on a stable landslide (i.e., that creeps continuously) in this study, it can also describe the motion of unstable landslides assuming $a < b$.

Based on our results, the analogy between creeping landslides and afterslip tectonic fault mechanics seems sound. Indeed, both dynamics are controlled by the perturbation by an earthquake of the sliding velocity of a creeping interface, assuming that rate and state friction governs the evolution of the frictional stress. A significant difference is that the postseismic displacement of a landslide can be much larger than the coseismic one as observed here, a feature not observed on tectonic faults. However, the amount of afterslip on active faults is only inferred by inversion of geodetic data and is not a reliable feature of the inversion [*Perfettini and Avouac*, 2014].

Slow-moving landslides can therefore be considered as a mechanical analogous of creeping faults. Their easier monitoring due to their smaller spatial scales, shallower characteristics, and faster kinematics makes landslides interesting candidates to study the frictional behavior of creeping zones of tectonic faults. This paper opens new perspectives to characterize rock friction at an intermediate scale between the laboratory and the active faults scale, a necessary feature to understand the complex dynamics of faulting and landslides.

Acknowledgments
This research was financially supported by the IRD and is part of the joint program IRD-INGEMMET. The Pléiades images have been provided by Astrium and the ISIS/CNES program. The GPS data are available for free on demand to the corresponding author. The authors acknowledge F. Bondoux and N. Cotte for their support with the GPS installation and processing, J. Jay for processing the InSAR, E. Berthier for his advises on the Pléiades processing, and J.L. Chatelain for the logistics. We are also grateful to the Maca authorities, school professors, and inhabitants who helps preserving the permanent instrumentation. This study also benefits from discussions with M. Bouchon, J.P. Avouac, and A. Walsperdorf.

Eric Calais thanks two anonymous reviewers for their assistance in evaluating this paper.

References

Agnesi, V., M. Camarda, C. Conoscenti, C. Di Maggio, I. Serena Diliberto, P. Madonia, and E. Rotigliano (2005), A multidisciplinary approach to the evaluation of the mechanism that triggered the Cerda landslide (Sicily, Italy), *Geomorphology*, *65*(1-2), 101–116, doi:10.1016/j.geomorph.2004.08.003.

Altamimi, Z., L. Métivier, and X. Collilieux (2012), ITRF2008 plate motion model, *J. Geophys. Res.*, *117*, B07402, doi:10.1029/2011JB008930.

Antayhua, Y., H. Tavera, I. Bernal, H. Palza, and V. Aguilar (2002), Localizacion hipocentral y caracteristicas de la fuente de los sismos de Maca (1991), Sepina (1992), and Cabanaconde (1998), Region del volcan Sabancaya, *Bol. Soc. Geol. Peru*, *93*, 63–72.

Boulton, C., B. M. Carpenter, V. Toy, and C. Marone (2012), Physical properties of surface outcrop cataclastic fault rocks, Alpine fault, New Zealand, *Geochem. Geophys. Geosyst.*, *13*, Q01018, doi:10.1029/2011GC003872.

Boulton, C., D. E. Moore, D. A. Lockner, V. G. Toy, J. Townend, and R. Sutherland (2014), Frictional properties of exhumed fault gouges in DFDP-1 cores, Alpine fault, New Zealand, *Geophys. Res. Lett.*, *41*, 356–362, doi:10.1002/2013GL058236.

Bulmer, M. H., A. Johnston, F. Engle, and G. Salas (1999), Seismically triggered slope failures in the Colca Valley, Southern Peru, *EOS Trans. AGU*, *H41A-07*, S127.

Chau, K. T. (1995), Landslides modeled as bifurcations of creeping slopes with nonlinear friction law, *Int. J. Solids Struct.*, *32*(23), 3451–3464, doi:10.1016/0020-7683(94)00317-P.

Cruden, D., and D. L. Varnes (1996), Landslide types and processes, in *Landslides: Investigation and Mitigation*, edited by R. K. Turner and R. L. Schuster, pp. 36–75, National Academy Press, Washington, D. C.

Dadson, S. J., et al. (2004), Earthquake-triggered increase in sediment delivery from an active mountain belt, *Geology*, *32*(8), 733–736, doi:10.1130/G20639.1.

Dieterich, J. H. (1981), Constitutive properties of faults with simulated gouge, in *Mechanical Behavior of Crustal Rocks: The Handin Volume, Geophys. Monogr. Ser.*, vol. 24, edited by N. L. Carter et al., pp. 103–120, AGU, Washington, D. C.

Dorbath, L., A. Cisternas, and C. Dorbath (1990), Assessment of the size of large and great historical earthquakes in Peru, *Bull. Seismol. Soc. Am.*, *80*(3), 551–576.

Gomez, J. C., F. Audemard, and J. Quijano (2002), Efectos geologicos asociados al sismo del 23 de junio del 2001 en el sur del Peru, in *Terremoto de la region sur del Peru del 23 Junio de 2001*, pp. 159–174, Sociedad Geologica del Peru, Lima, Peru.

Hadley, J. (1960), Landslides and related phenomena accompanying the Hebgen Lake earthquake, *U. S. Geol. Surv. Prof. Pap. 435-K*, U. S. Gov. Printing Off., Washington, D. C.

Harp, E. L., and R. W. Jibson (1995), Seismic instrumentation of landslides: Building a better model of dynamic landslide behavior, *Bull. Seismol. Soc. Am.*, *85*(1), 93–99.

Herring, T., R. King, and S. McClusky (2010), GAMIT reference manual: GPS analysis at MIT, release 10.4.

Hsu, Y.-J., M. Simons, J.-P. Avouac, J. Galetzka, K. Sieh, M. Chlieh, D. Natawidjaja, L. Prawirodirdjo, and Y. Bock (2006), Frictional afterslip following the 2005 Nias-Simeulue earthquake, Sumatra, *Science*, *312*(5782), 1921–1926, doi:10.1126/science.1126960.

Huang, R., and X. Fan (2013), The landslide story, *Nat. Geosci.*, *6*(5), 325–326, doi:10.1038/ngeo1806.

Ikari, M. J., D. M. Saffer, and C. Marone (2009), Frictional and hydrologic properties of clay-rich fault gouge, *J. Geophys. Res.*, *114*, B05409, doi:10.1029/2008JB006089.

Jibson, R. W., C. S. Prentice, B. A. Borissoff, E. A. Rogozhin, and C. J. Langer (1994), Some observations of landslides triggered by the 29 april 1991 Racha earthquake, republic of Georgia, *Bull. Seismol. Soc. Am.*, *84*(4), 963–973.

Keefer, D. K. (2002), Investigating landslides caused by earthquakes—A historical review, *Surv. Geophys.*, *23*(6), 473–510, doi:10.1023/A:1021274710840.

Lin, G.-W., H. Chen, Y.-H. Chen, and M.-J. Horng (2008), Influence of typhoons and earthquakes on rainfall-induced landslides and suspended sediments discharge, *Eng. Geol.*, *97*(1-2), 32–41, doi:10.1016/j.enggeo.2007.12.001.

Marone, C. (1998), Laboratory-derived friction laws and their application to seismic faulting, *Annu. Rev. Earth Planet. Sci.*, *26*(1), 643–696, doi:10.1146/annurev.earth.26.1.643.

Moro, M., M. Chini, M. Saroli, S. Atzori, S. Stramondo, and S. Salvi (2011), Analysis of large, seismically induced, gravitational deformations imaged by high-resolution COSMO-SkyMed synthetic aperture radar, *Geology*, *39*(6), 527–530, doi:10.1130/G31748.1.

Newmark, N. M. (1965), Effects of earthquakes on dams and embankments, *Geotechnique*, *15*(2), 139–159.

Niemeijer, A. R., and R. L. M. Vissers (2014), Earthquake rupture propagation inferred from the spatial distribution of fault rock frictional properties, *Earth Planet. Sci. Lett.*, *396*, 154–164, doi:10.1016/j.epsl.2014.04.010.

Perfettini, H., and J.-P. Avouac (2004), Postseismic relaxation driven by brittle creep: A possible mechanism to reconcile geodetic measurements and the decay rate of aftershocks, application to the Chi-Chi earthquake, Taiwan, *J. Geophys. Res.*, *109*, B02304, doi:10.1029/2003JB002488.

Perfettini, H., and J. P. Avouac (2014), The seismic cycle in the area of the 2011 Mw9.0 Tohoku-Oki earthquake, *J. Geophys. Res. Solid Earth*, *119*, 4469–4515, doi:10.1002/2013JB010697.

Petley, D., S. Dunning, N. Rosser, and A. Kausar (2006), Incipient earthquakes in the Jhelum valley, Pakistan following the 8th October 2005 earthquake, in *Disaster Mitigation of Debris Flows, Slope Failures and Landslides, Frontiers of Sci. Ser.*, vol. 47, edited by H. Marui, pp. 47–56, Universal Academy Press, Tokyo, Japan.

Pradel, D., P. M. Smith, J. P. Stewart, and G. Raad (2005), Case history of landslide movement during the Northridge earthquake, *J. Geotech. Geoenviron. Eng.*, *131*(11), 1360–1369, doi:10.1061/(ASCE)1090-0241(2005)131:11(1360).

Saffer, D. M., K. M. Frye, C. Marone, and K. Mair (2001), Laboratory results indicating complex and potentially unstable frictional behavior of smectite clay, *Geophys. Res. Lett.*, *28*(12), 2297–2300, doi:10.1029/2001GL012869.

Trifunac, M. D., and A. G. Brady (1975), A study on the duration of strong earthquake ground motion, *Bull. Seismol. Soc. Am.*, *65*(3), 581–626.

Wang, C.-Y., L.-H. Cheng, C.-V. Chin, and S.-B. Yu (2001), Coseismic hydrologic response of an alluvial fan to the 1999 Chi-Chi earthquake, Taiwan, *Geology*, *29*(9), 831–834, doi:10.1130/0091-7613(2001)029<0831:CHROAA>2.0.CO;2.

Wasowski, J., V. Pierri, P. Pierri, and D. Capolongo (2002), Factors controlling seismic susceptibility of the Sele valley slopes: The case of the 1980 Irpinia earthquake re-examined, *Surv. Geophys.*, *23*(6), 563–593, doi:10.1023/A:1021230928587.

Wilson, R. C., and D. K. Keefer (1983), Dynamic analysis of a slope failure from the 6 August 1979 Coyote lake, California, earthquake, *Bull. Seismol. Soc. Am.*, *73*(3), 863–877.

Zumberge, J. F., M. B. Heflin, D. C. Jefferson, M. M. Watkins, and F. H. Webb (1997), Precise point positioning for the efficient and robust analysis of GPS data from large networks, *J. Geophys. Res.*, *102*(B3), 5005–5017, doi:10.1029/96JB03860.

